

1 **Evaluating Snow Depth Measurements from Ground-Penetrating**
2 **Radar and Airborne Lidar in Boreal Forest and Tundra**
3 **Environments during the NASA SnowEx 2023 Campaign**

4 Kajsa Holland-Goon¹, Randall Bonnell^{2,1}, Daniel McGrath¹, W. Brad Baxter³, Tate Meehan⁴, Ryan
5 Webb⁵, Christopher F. Larsen⁶, Hans-Peter Marshall⁷, Megan Mason^{8,9}, Carrie Vuyovich⁸

6 ¹Department of Geosciences, Colorado State University, Fort Collins, Colorado, USA

7 ² U.S. Geological Survey, Water Resources Mission Area, Denver, Colorado, USA

8 ³Cold Regions Research and Engineering Laboratory, U.S. Army Corps of Engineers, Fairbanks, Alaska, USA

9 ⁴Cold Regions Research and Engineering Laboratory, U.S. Army Corps of Engineers, Hanover, New Hampshire, USA

10 ⁵Department of Civil and Architectural Engineering & Construction Management, University of Wyoming, Laramie,
11 Wyoming, USA

12 ⁶Geophysical Institute, University of Alaska, Fairbanks, Alaska, USA

13 ⁷Department of Geosciences, Boise State University, Boise, Idaho, USA

14 ⁸Hydrological Sciences Laboratory, NASA Goddard Space Flight Center, Greenbelt, Maryland, USA

15 ⁹Science Systems Applications Inc., Lanham, Maryland, USA

16 *Correspondence to:* Randall Bonnell (rbonnell@usgs.gov), Daniel McGrath (daniel.mcgrath@colostate.edu)

17

18 **Abstract.** We evaluated ground-penetrating radar (GPR) and airborne lidar retrievals of snow depth collected during the
19 NASA SnowEx 2023 campaign in tundra and boreal forest environments in Alaska along 44 short (3–12 m) transects.
20 Compared to in situ observations, we identified modest biases for GPR snow depths (bias <0.03 m in tundra, +0.06 m in boreal
21 forests) and larger biases for lidar snow depths in the boreal forests (–0.16 m). At the Upper Kuparuk-Toolik tundra site, lidar
22 snow depths exhibited a small bias (–0.02 m), whereas the bias was much larger at the Arctic Coastal Plain tundra site (+0.19
23 m). For most sites, biases were primarily related to sub-snow vegetation, tussocks, and seasonally dynamic ground. However,
24 we identified vertical alignment issues with the Arctic Coastal Plain lidar snow depth dataset that likely contributed to the
25 higher bias. The complex ground surface and sub-snow vegetation in these environments present a challenge to established
26 snow depth measurement methods, which needs to be considered when evaluating novel remote sensing approaches.

27 **1 Introduction**

28 In high-latitude (>60°) terrestrial systems, snow plays a crucial role in the hydrologic cycle and modulates the surface energy
29 balance. Snow strongly impacts the ecology of these regions: snow influences caribou winter range selection (Duquette, 1988;
30 Pedersen et al., 2021) and vegetation phenology (Kelsey et al., 2021), and provides winter refuges for a diverse range of
31 animals (Aitchison, 1987; Penczykowski et al., 2017). Snow cover extent in the Arctic has experienced dramatic reductions
32 during the satellite era, with observed declines of –3.5% and –13.4% per decade in May and June, respectively (Meredith et
33 al., 2019). Given the vast spatial scales and sparse in situ station network, remote sensing can play a critical role in snowpack
34 monitoring in these sensitive environments.

35 The NASA SnowEx 2023 campaign was implemented to improve the understanding of remote sensing methods for
36 retrievals of snow depth and snow water equivalent (SWE), the mass of the snowpack, in tundra and boreal forest environments
37 (Vuyovich et al., 2024). These regions are understudied relative to temperate mountains; for instance, they are currently not
38 included in gridded SWE analysis products (e.g., SNODAS). Space-borne remote sensing retrievals of snow depth or SWE at
39 high spatial resolution may be achievable in these complex environments through lidar or radar methods (Fair et al., 2025;
40 Eppler et al., 2022), but further evaluation of the uncertainties caused by the unique physical parameters within these
41 environments (e.g., dense canopy cover and ground vegetation) is required.

42 The boreal forest is characterized by a dense canopy of coniferous and deciduous trees and covers 10–17% of the world’s
43 landmass (NASA Earth Observatory, 2006; Vuyovich et al., 2024). Boreal forest seasonal snowpacks are typically shallow
44 (<1.2 m) and exhibit lower snow densities due to minimal wind loading, cold temperatures, and large temperature gradients in
45 the snowpack, resulting in extensive faceting (Pruitt, 1970). In contrast, the Arctic tundra extends to higher latitudes than
46 boreal forests and is subject to extreme cold temperatures and high winds that limit plant growth. Tundra snowpacks are
47 typically shallower than boreal forest snowpacks, but wind redistribution can build deep snow drifts (Benson, 1967; Benson
48 and Sturm, 1993). Because of wind-driven compaction, tundra snowpacks can exhibit higher densities than snowpacks in the
49 boreal forest and include a binary stratigraphy of high-density wind slab above low-density, large-grained depth hoar. Both

50 environments have features that may complicate snow depth retrievals from lidar or radar methods. In boreal forests, thick
51 forest canopy, canopy-intercepted snow, and dense shrub and tussock (i.e., small localized tufts of grass or sedge where the
52 solid ground is raised) cover may occlude lidar, whereas dense shrub cover can cause a void space between the bottom of the
53 snowpack and the ground, leading to a mismatch between the more easily identified radar ground reflector and the true base
54 of the snowpack. Tundra environments contain spatially varying distributions of shrub and tussock cover that may increase
55 uncertainty of lidar or radar methods. Additionally, the North Slope tundra ground surface is complex and experiences seasonal
56 fluctuations driven by freeze-thaw processes. These environments contain hummocks, ice wedges, ice polygons, and are
57 underlain by shallow permafrost (Jorgenson et al., 2008). This dynamic ground surface can increase lidar snow depth
58 uncertainty because of differences in the ground elevation between snow-on and snow-off lidar acquisitions (Chen et al., 2020).
59 In both environments, frozen soil may have similar dielectric properties to the snowpack, and thus the radar signal can penetrate
60 below the snow-ground interface.

61 During NASA SnowEx 2023 in Alaska, we conducted detailed in situ surveys to improve our understanding of radar and
62 lidar performance for snow depth retrieval in these complex high-latitude environments. Here, we evaluate ground-based radar
63 and airborne lidar snow depth products along transects where manual measurements of snow depth were collected after snow
64 excavation. The excavated snow depths represent the integrated thickness of the snowpack, which excludes intra- and sub-
65 snowpack void spaces. In particular, we emphasize how sub-snow vegetation and variable ground conditions associated with
66 mosses, tussocks, and/or permafrost influence the retrieval accuracy.

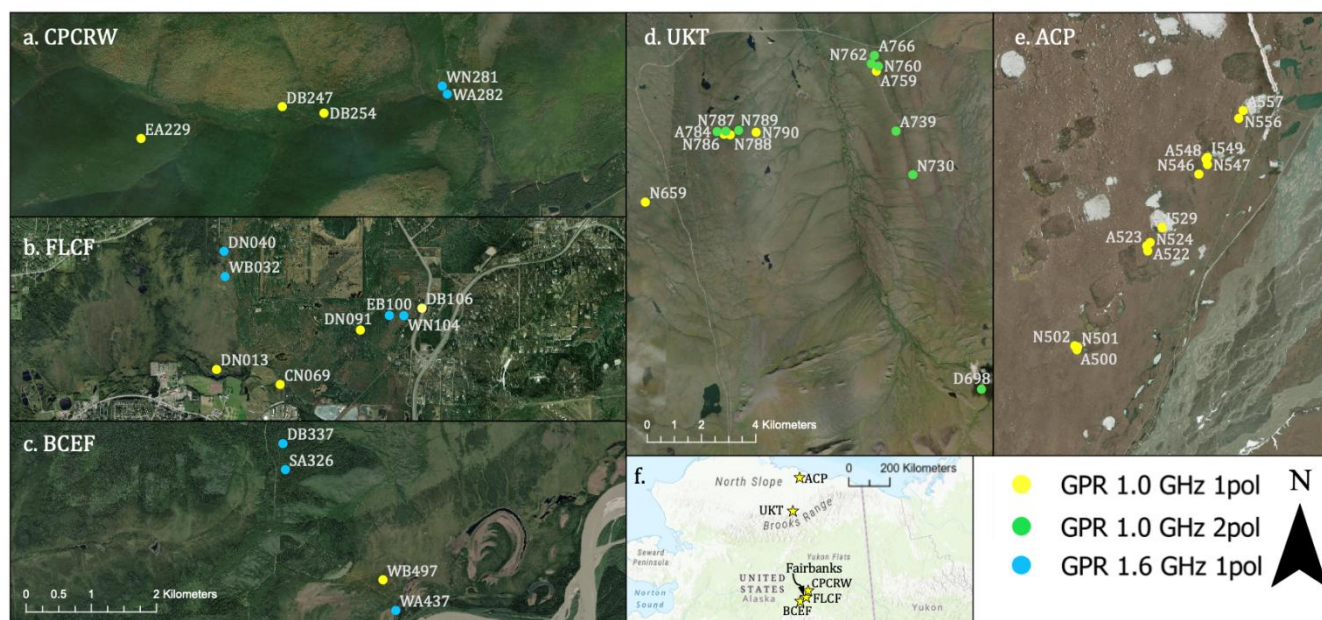
67

68 **2 Study Sites**

69 The NASA SnowEx 2023 Alaska campaign (7–16 March 2023) was operated at three field sites in the boreal forests near
70 Fairbanks (Figure 1a–c) and two sites in the Arctic tundra on the North Slope (Figure 1d, e). Although some snowmelt was
71 observed in the boreal forest canopy, the snowpack on the ground was considered dry based on snow pit temperature
72 measurements. Of the boreal forest sites, the Caribou/Poker Creek Research Watershed site (CPCRW; Figure 1a) is located
73 ~25 km northeast of Fairbanks and hosted eight surveys, the Farmers Loop Experimental Station and Creamer’s Field
74 Migratory Waterfowl Refuge (FLCF; Figure 1b) north of Fairbanks hosted six surveys, and the Bonanza Creek Experimental
75 Forest (BCEF; Figure 1c) is ~20 km southwest of Fairbanks and hosted four surveys. Vegetation varied by site: CPCRW
76 surveys were performed primarily below black spruce canopy, FLCF included transects within black spruce (*Picea mariana*),
77 deciduous, mixed canopy, and agricultural field environments, and BCEF surveys were performed primarily below leaf-off
78 deciduous canopy and in wetland shrub environments (Vuyovich et al., 2024). Surveys at the Upper Kuparuk-Toolik site
79 (UKT; Figure 1d) had ground conditions that varied from shrubs and tussocks to frozen ponds, whereas the Arctic Coastal
80 Plain site (ACP; Figure 1e), located near Deadhorse, primarily included surveys performed in wetlands and frozen ponds/lakes

81 (Vuyovich et al., 2024). The sites near Fairbanks are within the discontinuous permafrost region (Jorgenson et al., 2008),
82 whereas both UKT and ACP are underlain by continuous permafrost (Obu et al., 2019).

83



84

85

86 **Figure 1: Ground surveys at the (a) Caribou/Poker Creek Research Watershed (CPRW), (b) Farmers Loop/Creamer's Field**
87 **(FLCF), (c) Bonanza Creek Experimental Forest (BCEF), (d) Upper Kuparuk-Toolik (UKT), and (e) Arctic Coastal Plain (ACP)**
88 **field sites. (f) Map inset depicts the locations of the five field sites within Alaska. Imagery provided by ESRI, Maxar and Microsoft.**

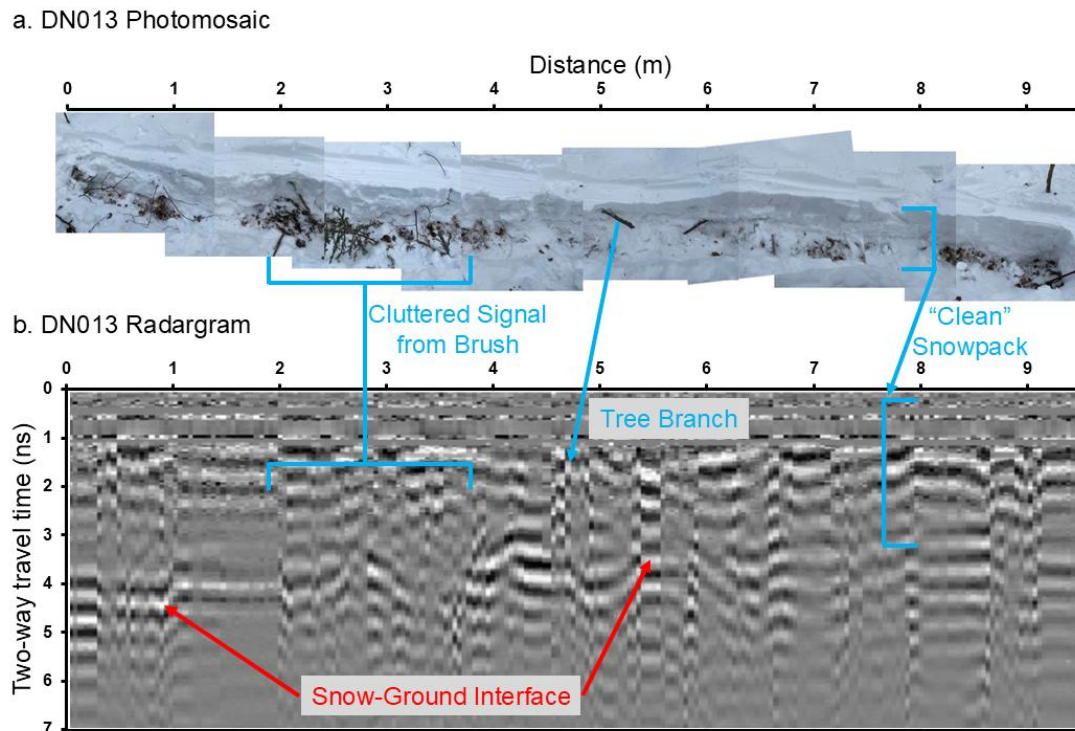
89 3 Methods

90 3.1 Summary of Field and Airborne Lidar Surveys

91 We operated four ground-penetrating radar (GPR) systems to cover the five field sites, including two surface-coupled 1.0 GHz
92 center-frequency PulseEkko Pro single transceiver/receiver systems, an air-coupled 1.0 GHz center-frequency PulseEkko Pro
93 single transceiver with dual polarization receivers system, and a surface-coupled 1.6 GHz GSSI single transceiver/receiver
94 system. The PulseEkko Pro systems have a 6 dB bandwidth of 500–1500 MHz, whereas the GSSI system has a 6 dB bandwidth
95 of 800–2400 MHz. Each GPR used a GNSS system to provide locations for collected traces: the air-coupled PulseEkko Pro
96 used a Geode dGPS system (± 0.5 m accuracy), the two sled-coupled PulseEkko Pro GPRs used Emlid RS2 rovers with Emlid
97 RS2 bases located nearby for post-kinematic processing (± 0.5 m accuracy), and the sled-coupled GSSI GPR used a mapping-
98 grade GPS system (± 3 m accuracy). In Figure 1, each transect is marked by the associated GPR system.

99 For the three surface-coupled GPR surveys, the GPR was pulled across the surface of the snowpack in a sled, whereas the
100 air-coupled GPR was carried by two people above the snow surface. GPR systems were operated in the common-offset

101 configuration and we took care not to disturb the snowpack immediately below the GPR transect. Transect lengths ranged
102 from 3–12 m. Methods for deriving GPR snow depths are provided in Section 3.2. Following GPR data collection, the snow
103 along the full length of the transect was excavated and snowpack thicknesses, which excluded any void spaces or tree branches
104 or logs in the snowpack, were measured at 0.25–1 m intervals. A recent study supports this methodology because void spaces
105 can be identified and subtracted from the measured depths (Stuefer et al., 2025). Pictures and/or video recordings were acquired
106 for each transect and detailed notes were taken on vegetation and ground conditions. An example photomosaic of an excavated
107 boreal forest transect is provided in Fig. 2. Each survey was completed within 15 m of a snow pit, wherein measurements of
108 snow depth, snow density, SWE, and snow temperature were collected. In total, 17 surveys were collected at the boreal forest
109 field sites and 27 surveys were collected at the tundra field sites on the North Slope. At each field site, snow-on airborne lidar
110 surveys were collected during the campaign and snow-off airborne lidar surveys were collected during the following summer.
111 Snow-on and snow-off lidar surveys were used to generate 0.5 m snow depth and canopy height models (Larsen, 2024). We
112 note that lidar-derived snow depths based on acquisitions that occurred before or after ground surveys have increased
113 uncertainty due to either a changed snow surface (i.e., accumulation, compaction, redistribution) between the lidar flights and
114 ground surveys or snow disturbance caused by the ground observations that preceded lidar flights (n = 20/44). Further
115 processing details for the lidar snow depths are provided in Larsen (2024). A list of lidar and ground survey dates is provided
116 in Table 1 and snow accumulation measurements for every day of the campaign are provided in Table S1.
117



118

119

120

121 **Figure 2: (a) Photomosaic and corresponding (b) radargram of the 9.5 m long DN013 transect from 7 March 2023 in Farmers**
 122 **Loop/Creamers Field. Annotations illustrate the complexities of GPR collection in the dense brush of boreal forests. In particular,**
 123 **we show the signal clutter caused by intra-snowpack vegetation, signal ringing that results from tree branches or tree trunks, snow**
 124 **stratigraphy in areas without vegetation (“clean” snowpack), and the location of the snow-ground interface, which ranges from ~4**
 125 **ns near 0 m distance to ~3 ns near 9 m distance.**

126

127

128 **Table 1: Summary of field and airborne survey dates.**

	Field Site	Snow-On Lidar Flight Dates	Ground Survey Dates	Transects (n)
Tundra	Arctic Coastal Plain	10 March 2023	11–14 March 2023	13
	Upper Kuparuk- Toolik	13 March 2023	8–11, 15 March 2023	14
Boreal Forest	Farmers Loop/ Creamers Field	11 March 2023	7–11, 13 March 2023	8
	Bonanza Creek Experimental Forest	11 March 2023	10, 13–15 March 2023	4
	Caribou/Poker Creek Research Watershed	11 March 2023	8–9, 11, 14 March 2023	5

129

130 **3.2 Ground-Penetrating Radar Processing and Sources of Snow Depth Uncertainty**

131 For GPR systems, the transceiver emits a signal that transmits through the snowpack and reflects off boundaries of contrasting
 132 dielectric permittivities (e.g., vegetation, snow stratigraphy, the snow-ground interface). The receiver then records the
 133 amplitude and two-way travel times (*twtt*) of these reflections. Radargrams were processed to a trace spacing of ~0.10 m. We
 134 provide an example of a boreal forest radargram in Fig. 2.

135 Exported *twtt* of the snow-ground interface, typically identified as the first reflection at depth with the highest amplitude
 136 that is spatially coherent, were manually selected for all single-polarization GPR datasets (e.g., McGrath et al., 2019). For the
 137 dual-polarization GPR dataset, *twtt* was obtained by utilizing the coherent reflection between the two receivers (further details

138 provided in Meehan et al., 2024). The $twtt$ can be converted to snow depth with an estimate of the snowpack radar velocity
139 (v_s ; Daniels, 2004)

$$140 \quad v_s = \frac{c}{\sqrt{\varepsilon_s}}, \quad (1)$$

141 where c is the speed of electromagnetic energy in a vacuum and ε_s is the dielectric permittivity of the snowpack. Snowpack
142 conditions were dry during our surveys, thus, the relative permittivity can be approximated from the bulk snow density (ρ_s)
143 through an empirical relation (Kovacs et al., 1995)

$$144 \quad \sqrt{\varepsilon_s} = 1 + \frac{0.845 \times \rho_s}{1000}. \quad (2)$$

145 Snow density was sampled in snow pits adjacent to the surveyed transects using 1000 cm³ wedge samplers at 10 cm intervals
146 along two columns in the snow pit. If density measurements differed by more than 10% for a single layer, a third measurement
147 was acquired. For layers with three measurements, we excluded the measurement with the largest difference. We then
148 calculated bulk snow densities as the column average. Finally, snow depth (D_s) is calculated as

$$149 \quad D_s = \frac{twtt}{2} \times v_s. \quad (3)$$

150

151 GPR surveys have several sources of uncertainty. GNSS positioning was estimated as ± 0.5 – 3 m horizontal accuracy at
152 the boreal forest sites and ± 0.5 m at the Arctic tundra sites, which could complicate the comparison between GPR and lidar
153 snow depths. GPR-derived snow depths may be reduced by up to 0.07 m due to removal and/or compaction of snow as the
154 sled travels across the surface. Finally, site-specific ground conditions may add uncertainty to the GPR snow depths. A few
155 examples include: (1) snow depths may be overestimated because of the presence of void spaces within the snowpack caused
156 by vegetation, (2) snow depths may be underestimated when a dense layer of vegetation obscures the true bottom of the
157 snowpack (e.g., a buried bent-over tree), and (3) snow depths may be overestimated if the radar signal penetrates into frozen
158 soil without a strong reflection at the snow-ground interface.

159 **3.3 Evaluation of GPR and Lidar Snow Depths**

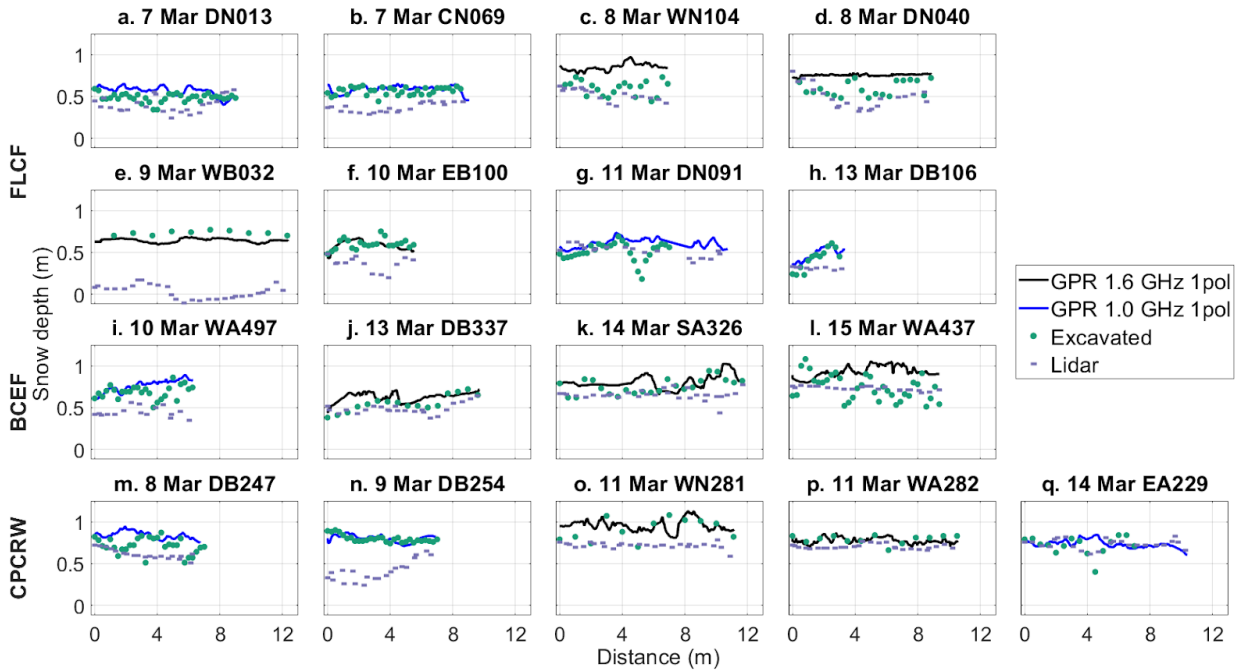
160 We extracted the lidar snow depths (0.5 m x 0.5 m resolution) along each surveyed transect based on the GNSS coordinates
161 recorded by the GPR. We aligned the excavated depth locations with the GPR depth locations based on field measurements,
162 resulting in a high-quality co-registration between the GPR and the excavated depths. However, the co-registration between
163 the lidar data and the transect surveys are subject to the GNSS uncertainty listed above. GPR, lidar, and excavated depths were
164 then compared as individual profiles to evaluate any systematic differences. We calculated the mean and standard deviation of
165 snow depth for the GPR, lidar, and in-situ measurements from each transect to estimate the overall root mean squared error
166 (RMSE), bias, and Pearson's correlation coefficient (r) between measurement techniques in both the tundra and boreal forest
167 sites. Although both GPR and lidar snow depths likely contain errors and biases, we primarily emphasize bias in the results and
168 discussion because the two are difficult to untangle due to the complex conditions in which these data were collected. Finally,

169 lidar-derived vegetation heights were extracted along each transect in the boreal forest to determine whether accuracy was
170 related to lidar-derived vegetation height.

171 **4 Results**

172 **4.1 Boreal Forest Transects**

173 At boreal forest sites, GPR mean snow depths overestimated excavated mean snow depths for 12 of 17 transects, whereas lidar
174 mean snow depths underestimated excavated mean snow depths for 14 of 17 transects (Table S2, Figure 3). Large differences
175 (>0.20 m) between GPR and excavated depths occurred where sub-snow shrubs or tree branches caused void spaces in the
176 snowpack (e.g., Figure 3g, i), but close agreement was observed for the transect in the agricultural field where only crop stubble
177 was present below the snowpack (Figure 3b) and for transects below black spruce canopy (e.g., Figure 3n–p). The average
178 residual between GPR and excavated depths was $+0.06$ m (9% of mean excavated depth) and the average residual between
179 lidar and excavated depths was -0.12 m (16% of overall mean excavated depth) when field surveys occurred after lidar
180 acquisitions (Table S2). For these surveys, the lidar profile either mostly mimicked the excavated depths and agreed within
181 ± 0.07 m (e.g., Figure 3j, 3p), or the lidar profile failed to capture both the spatial patterns and exhibited reduced accuracy when
182 compared to the excavated depths (e.g., Figure 3h, 3l). The lidar snow depth bias worsened to -0.16 m (24% of mean excavated
183 depth; Table S2) when surveys performed before the lidar survey date were included in the comparison. We visually inspected
184 the boreal forest lidar snow depth rasters to verify the presence of all transects excavated before the 11 March lidar survey and
185 we found that excavation activities clearly influenced five of these surveys. These transects are shown in Fig. 3b, 3d, 3e, 3f,
186 and 3n, illustrating how sample timing can severely bias direct comparisons between field and remote sensing-based depth
187 estimates.



188

189

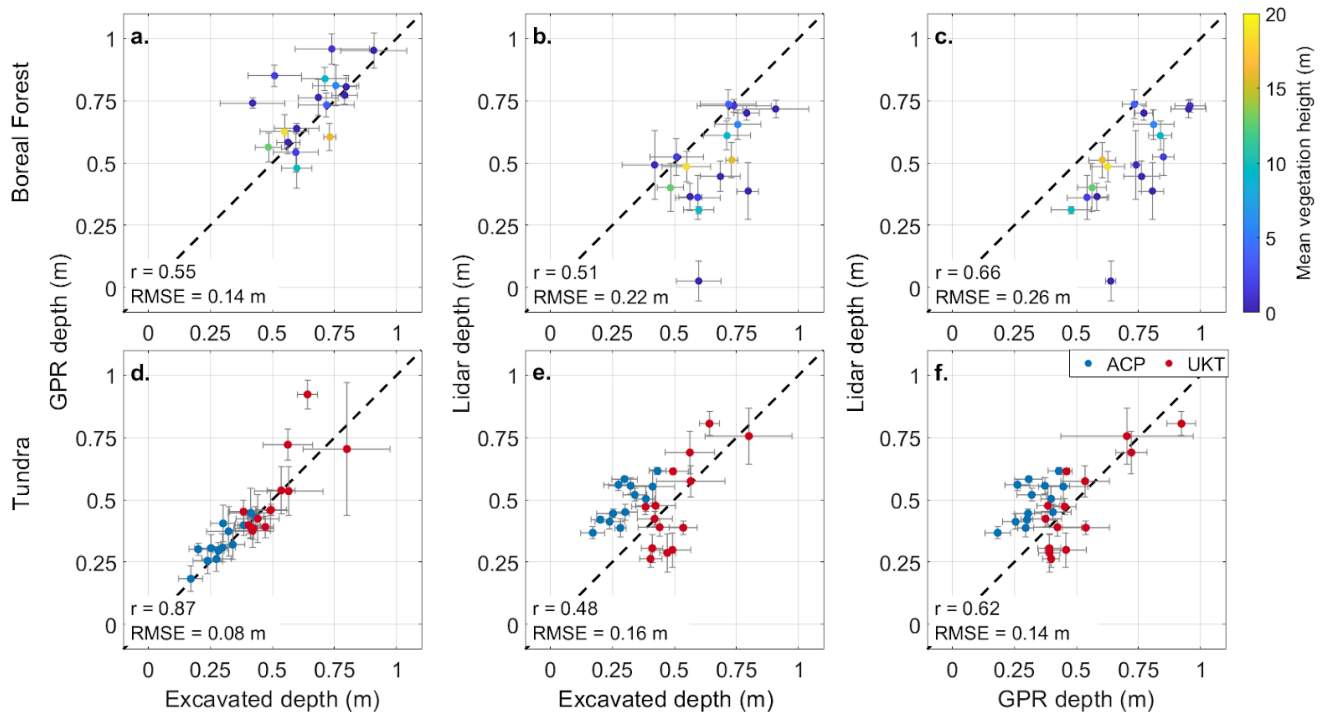
Figure 3: Snow depth profiles at the boreal forest for the (a–h) Farmer’s Loop/Creamer’s Field (FLCF), (i–l) Bonanza Creek Experimental Forest (BCEF), and (m–q) Caribou/Poker Creek Research Watershed (CPCRW) field sites. GPR snow depth profiles were collected by the 1.6 GHz GPR system and the 1.0 GHz GPR system. Subplots are labeled by transect numbers. Airborne lidar surveys were conducted at all three sites on 11 March 2023.

193

194

Of the three boreal forest field sites, CPCRW yielded the lowest mean GPR residual (+0.03 m), whereas BCEF yielded the highest mean residual (+0.11 m). Three of the five CPCRW transects were performed below black spruce canopy, where mosses are the dominant substrate and shrub canopy is sparse, whereas shrubs and tussocks dominate the ground below BCEF transects. FLCF surveys (mean GPR residual = +0.06 m) were performed primarily below mixed deciduous/coniferous canopy and contained various shrubs, saplings, and tree branches within the snowpack. Compared to GPR, mean lidar residuals exhibited the opposite canopy-driven trend; BCEF surveys yielded the lowest mean residuals (−0.10 m) and FLCF/CPCRW yielded the highest mean residuals (−0.19 m and −0.15 m). However, we note that three of four BCEF surveys were performed after lidar collection, whereas eight of 13 surveys at FLCF/CPCRW were performed before lidar collection (Table S2). Overall, we calculated an r of 0.55 and RMSE of 0.14 m for GPR snow depths and an r of 0.51 and RMSE of 0.22 m for lidar snow depths at the boreal forest field sites (Figure 4a–b). The best Pearson’s correlation coefficient, but highest RMSE was observed for the lidar vs. GPR comparison ($r = 0.66$, RMSE = 0.26 m; Figure 4c).

205



206

207

208

209

210

211

212

Figure 4: Comparisons at the boreal forest (a–c) and tundra sites (d–f) between (a, d) GPR and excavated depths, (b, e) lidar and excavated depths, and (c, f) lidar and GPR depths. The mean values are plotted with error bars calculated from the standard deviation. Points in a–c are colored by mean lidar-derived vegetation height, which represents the canopy height in forest cover or the shrub/grass height in meadows. Points in d–f are colored by field site. Sites: ACP, Arctic Coastal Plain; UKT, Upper Kuparuk-Toolik.

213

4.2 Tundra Transects

214

215

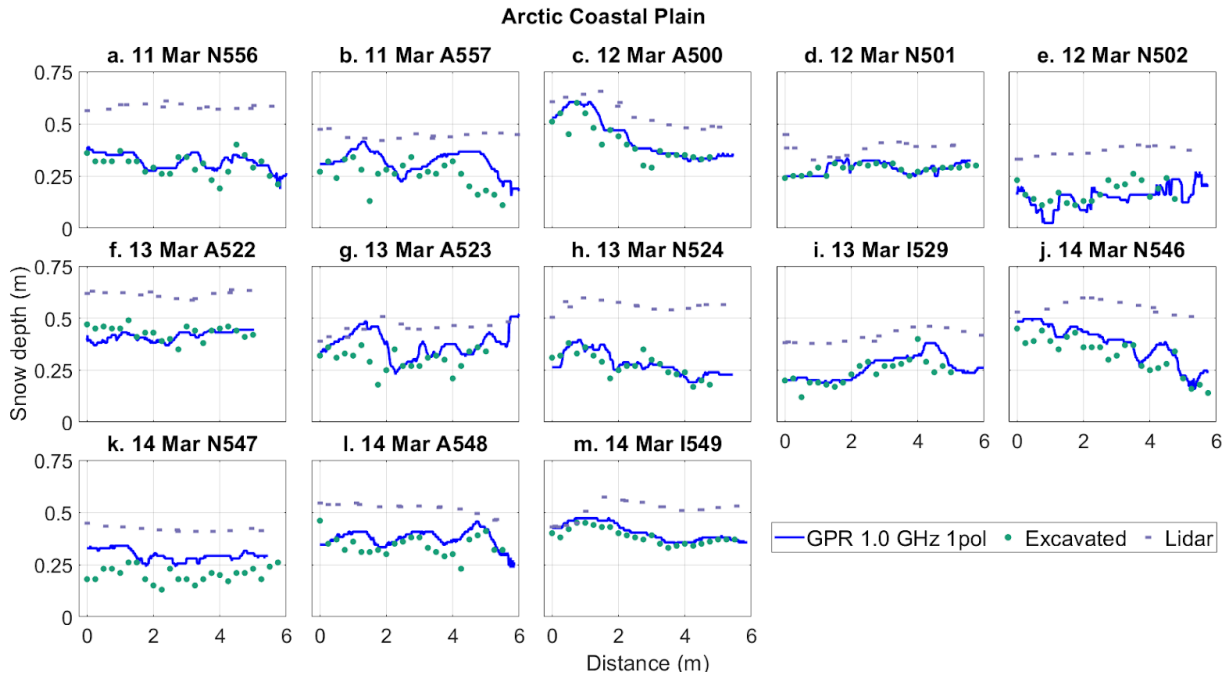
216

217

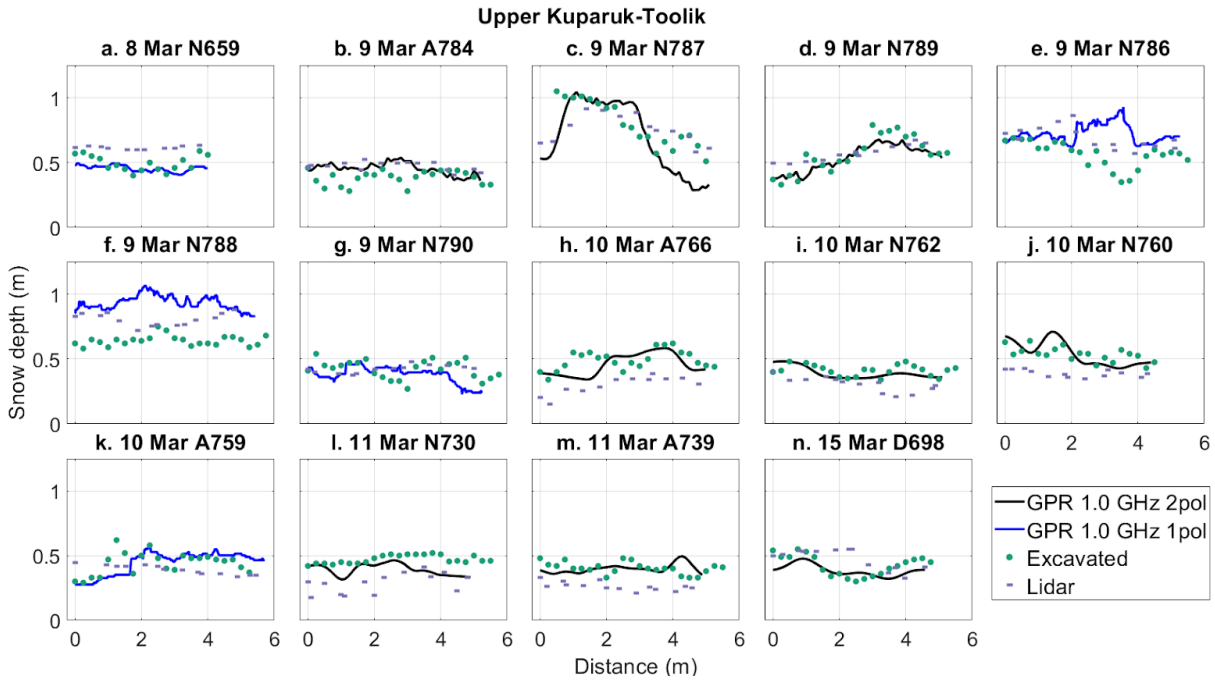
218

219

Vegetation structure was less complex at the Arctic tundra sites than at the boreal forest sites. At ACP, surveys had grassy ground cover (11 surveys with grass heights of 0.05–0.20 m) or ground ice (two surveys; Figure 5i, m), whereas tussocks (four surveys with tussock heights of 0.08–0.25 m) and shrubs (four surveys with shrub heights <0.30 m) were the predominant ground cover at UKT. Based on the excavated depths, both mean GPR residuals (ACP = +0.03 ± 0.04 m; UKT = +0.01 ± 0.10 m; Tables S3–S4, Figures 5–6) and the overall performance metrics ($r = 0.87$; RMSE = 0.08; Figure 4d) improved at the Arctic tundra sites relative to the boreal forest sites.



220
 221 **Figure 5: Snow depth profiles at the Arctic Coastal Plain tundra field site organized by date and transect number. GPR snow depth**
 222 **profiles were collected by the single-polarization 1.0 GHz GPR system. Airborne lidar survey was conducted on 10 March 2023.**
 223



224

225 **Figure 6: Snow depth profiles at the Upper Kuparuk-Toolik tundra field site organized by date and transect ID. GPR snow depth**
226 **profiles were collected by the single-polarization 1.0 GHz GPR system and the dual-polarization 1.0 GHz GPR system. Airborne**
227 **lidar survey was conducted on 13 March 2023.**

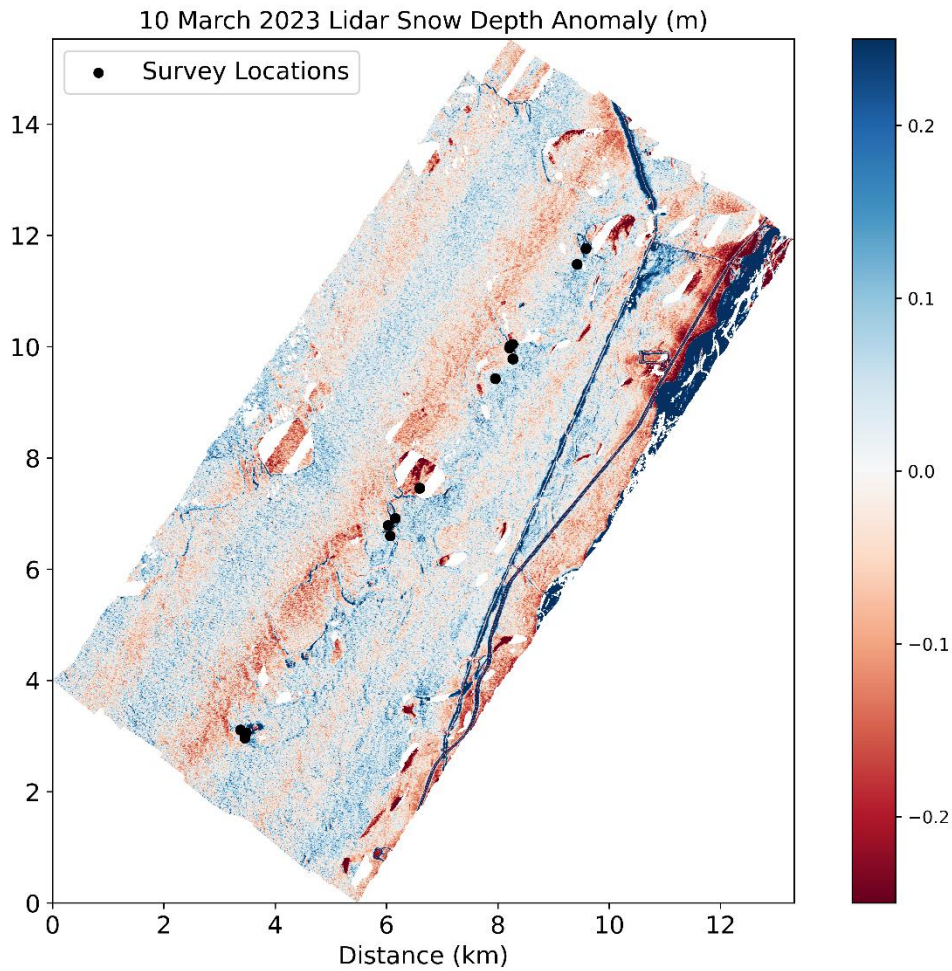
228
229 Compared to the boreal forest sites, the lidar snow depths from the Arctic tundra sites yielded a comparable Pearson's
230 correlation coefficient, but an improved RMSE ($r = 0.48$; $RMSE = 0.16$ m; Figure 4e). Despite having more complex ground
231 conditions than ACP, UKT yielded the lowest mean lidar residual (ACP = $+0.19 \pm 0.05$ m; UKT = -0.02 ± 0.12 m; Tables S3–
232 S4, Figures 5–6). All ACP lidar profiles exhibited poor magnitude agreement with the excavated depths. Despite this, several
233 of these profiles exhibited spatial patterns that were similar to the excavated depth profiles (Figures 5c, 5f, 5i, 5m) Notably,
234 all ACP surveys were performed after the lidar flight, whereas 13 of 14 UKT surveys preceded the lidar flight (Table 1). We
235 visually inspected the transects in the UKT lidar snow depth raster and observed that only five transects were influenced by
236 snow excavation (Figures 6h–j, 6l–m).

237 **5 Discussion**

238 **5.1 GPR and Lidar Snow Depth Uncertainty in Boreal Forest and Arctic Tundra Environments**

239 We found that GPR captured snow depth variability in both boreal forest and Arctic tundra environments over length scales
240 >0.5 m, but we observed larger uncertainty over shorter length scales (<0.5 m), likely due to the large sensor footprint (~ 1.5
241 m radius for a snow depth of 0.6 m; e.g., Daniels, 2004). GPR snow depths exhibited a modest positive bias ($+0.06$ m) relative
242 to excavated depths in the boreal forest and a smaller positive bias in the Arctic tundra (overall mean residuals = $+1$ – 3 cm;
243 Tables S2, S3). While it is possible that a portion of the observed GPR bias could be explained by differences between the
244 GPR and excavated depth measurement footprints, we largely attribute the positive biases to discontinuous vegetation-induced
245 void spaces at the base and within the snowpack (e.g., Figure 2; Berezovskaya and Kane, 2007). Vegetation was dense and
246 complex in the boreal forest, resulting in cluttered radargrams that were difficult to interpret, whereas Arctic tundra sites had
247 less complex vegetation and better-defined ground reflectors.

248 Lidar at ACP was expected to have the highest agreement with excavated depths because the lidar surveys were conducted
249 before the snowpack was disturbed. Instead, ACP lidar exhibited a $+0.19$ m average bias and failed to reproduce fine-scale
250 snow depth patterns (e.g., Figure 5a–b), despite having relatively simpler ground conditions at the time of the surveys. We
251 attribute this to a strip alignment issue in the ACP bare earth elevation model collected in August 2022, which results in linear
252 striping in the snow depths aligned with the lidar swaths. All ground surveys happened to be conducted within a single swath
253 that exhibited higher snow depths (Figure 7), which provides the likely explanation for the observed ACP bias in the snow
254 depths.



256
257
258
259 **Figure 7: Lidar snow depth anomalies at ACP with snow depth anomaly saturated between -0.25 and +0.25 m to illustrate the**
260 **linear lidar artifacts oriented southwest to northeast. All GPR transect locations are located within a single swath of the scene.**

261 Although UKT lidar exhibited lower mean bias, it also did not reproduce fine-scale snow depth patterns (e.g., Figure 6e–
262 f). Both ACP and UKT received <0.06 m of snow depth accumulation between ground-based and airborne surveys (Table S1).
263 Based on field observations, blowing snow and wind redistribution (e.g., Pomeroy and Li, 2000) likely caused the poor spatial
264 pattern agreement between excavated depth and lidar depth profiles. Seasonal thaw, which has been observed to drive
265 subsidence up to 0.05 m in this region (Chen et al., 2020), may also contribute, but is challenging to quantify with available
266 observations.

267 Lidar at the boreal forest also exhibited higher uncertainties, yielding an RMSE that was nearly half of the average
268 measured snow depth. However, May et al. (2025) demonstrated that the RMSE could be reduced to 0.12 m at CPRW by

269 removing anomalous snow depths and areas with anomalous snow depth patterns. Uncertainties tended to be higher for taller
270 vegetation heights (>5 m; Figure 4b), although we note a large range of accuracy for lower vegetation heights (<5 m). This
271 weaker agreement could be due to one or more of four primary factors: (1) snow disturbance due to ground surveys caused
272 errors within the lidar retrieval method, (2) differences in canopy structure between summer and winter acquisitions (e.g., bent-
273 over trees from snow burden), (3) signal penetration through the dense canopy may be problematic for the method (e.g.,
274 Hopkinson et al., 2004), or (4) GNSS location uncertainty between the lidar and excavated depths. Despite the higher
275 uncertainty for the lidar snow depths, the lidar coverage is spatially continuous and complete over the field sites, a clear
276 advantage over the GPR measurements.

277 **5.2 Implications for SnowEx23 GPR and Lidar Datasets**

278 Although we identified a clear bias for GPR in the boreal forest, it appears that this bias exhibited some dependence upon the
279 land cover, but we were unable to fully evaluate this point. Further work, potentially through a depth probe-GPR evaluation,
280 is needed to identify systematic biases within the boreal forest for GPR operation.

281 ACP lidar snow depths appear to be affected by swath alignment artifacts, which users should be aware of before using
282 the dataset. If the identified bias is removed from the lidar swath by simple subtraction, the ACP lidar RMSE improves from
283 0.20 m to 0.05 m. However, the remaining lidar swaths may be challenging to correct given the lack of independent in situ
284 observations in these swaths. At UKT, lidar snow depths exhibited low bias and relatively high accuracy, whereas lidar snow
285 depths at the boreal forest sites exhibited a substantial positive bias. Fair et al. (2025) evaluated ICESat-2 lidar snow depths at
286 UKT and FLCF using the airborne lidar snow depths and found better ICESat-2 performance at UKT ($r^2 = 0.84\text{--}0.92$) than at
287 FLCF ($r^2 = 0.14\text{--}0.58$), further highlighting the boreal forest complexities. In the forests, the lidar snow depth bias is directly
288 related to potential void spaces caused by shrub canopy interception and a lack of photon penetration below canopy and
289 underbrush. In the Arctic tundra, lidar snow depths may be influenced by seasonal thaw cycles. Given the magnitude of snow
290 disturbance associated with in situ surveys, we expect poor agreement between snow pit/excavated measurements and lidar
291 measurements when the field survey preceded the lidar flight (e.g., Figure 3e, n).

292 **6 Conclusions**

293 Snow is a critical component of the hydrology and ecology of high-latitude terrestrial environments, but distributed snow
294 depths are difficult to measure at high spatial resolution. As part of the NASA SnowEx March 2023 campaign, spatially
295 distributed L-band center-frequency GPR and airborne lidar data were collected and we evaluated snow depth retrievals at the
296 boreal forest and Arctic tundra sites. Biases were observed for both methods and in both environments. GPR surveys yielded
297 accurate snow depths, but with lower variability along the profile which was likely caused by the much larger footprint of the
298 radar signal. GPR, particularly when operated at or near the snowpack surface, is less sensitive to vegetation and snowpack
299 void spaces than the airborne lidar DEM differencing method. The timing of the lidar flights relative to ground surveys

300 complicated our evaluation, but we noted lower accuracy in the boreal forest that may have been caused by vegetation
301 preventing the lidar pulse from reaching the bare earth. Although lidar yielded accurate snow depths at the UKT site, we
302 identified vertical alignment issues that contributed to a large positive bias at ACP (bias = +0.19 m). The complex surface
303 conditions of the boreal forest and tundra regions challenge established snow observing methods, warranting careful
304 consideration when using these to evaluate novel remote sensing approaches.
305

306 **Author contributions**

307 Conceptualization: D.M., H.P.M., C.V., K.H.G., R.B., T.M., R.W. Data Curation: K.H.G., C.L., R.W., T.M., M.M., R.B.,
308 D.M., B.B. Analysis: K.H.G., R.B., T.M., R.W. Funding Acquisition: D.M., C.V., H.P.M., R.W., R.B., B.B., T.M., K.H.G.
309 Investigation: all authors. Methodology: K.H.G., D.M., T.M., R.W., R.B. Visualization: K.H.G, R.B. Writing – Original Draft
310 Preparation: K.H.G, R.B., D.M. Writing – Review & Editing: all authors.

311 **Acknowledgements**

312 K.H.G was supported by the Colorado State University Honors program. R.B. was supported by NASA FINESST award
313 80NSSC20K1624 and the U.S. Geological Survey Mendenhall Postdoctoral Fellowship Program. D.M., H.P.M., and R.W.
314 were supported by NASA THP award 80NSSC22K1113. We thank Dr. E. Baker, H. Flynn, and N. Latysh for providing
315 insightful comments which improved the clarity of this paper. Any use of trade, firm, or product names is for descriptive
316 purposes only and does not imply endorsement by the U.S. Government.

317 **Data Availability**

318 Boreal Forest GPR transects (Bonnell et al., 2025; <https://doi.org/10.5067/3X5Q3X7Y87U3>), Arctic Tundra dual polarization
319 GPR transects (Meehan and Rowland, 2024; <https://doi.org/10.5067/TSU0U7L4X2UW>) and single polarization (Webb, 2024;
320 <https://doi.org/10.5067/H3D9IT1W6JT6>), lidar data (Larsen, 2024; <https://doi.org/10.5067/BV4D8RRU1H7U>), and snow pits
321 (Mason et al., 2024; <https://doi.org/413819/SJZ90KNPKCYR>) are archived with the NSIDC DAAC. Creamer’s Field
322 SNOTEL data are available at <https://wcc.sc.egov.usda.gov/nwcc/site?sitenum=1302>. NOAA AK Deadhorse 3 S weather
323 station data are available at <https://www.ncei.noaa.gov/access/crn/sensors.htm?stationId=1793>.
324

325 **Competing Interests**

326 At least one of the (co-) authors is a member of the editorial board of *The Cryosphere*. The authors have no other competing
327 interests to declare

328 **References**

329 Aitchison, C. W.: Winter energy requirements of soricine shrews, *Mammal Review*, 17, 25-38, [https://doi.org/10.1111/j.1365-](https://doi.org/10.1111/j.1365-2907.1987.tb00046.x)
330 [2907.1987.tb00046.x](https://doi.org/10.1111/j.1365-2907.1987.tb00046.x), 1987

331 Benson, C. S.: Polar regions snow cover, *Physics of Snow and Ice: Proceedings*, 1, 1039-1063, 1967.

332 Benson, C. S. and Sturm, M.: Structure and wind transport of seasonal snow on the Arctic slope of Alaska, *Annals of*
333 *Glaciology*, 18, <https://doi.org/10.3189/S0260305500011629>, 1993.

334 Berezovskaya, S. and Kane, D. L.: Measuring snow water equivalent for hydrological applications: part 1, accuracy
335 observations, 16th International Northern Research Basins Symposium and Workshop, Petrozavodsk, 29-2007.

336 Bonnell, R., McGrath, D., Detre, A., and Holland-Goon, K.: SnowEx23 Mar23 IOP CSU 1 GHz Ground Penetrating Radar
337 Raw, Version 1 [data set], NASA National Snow and Ice Data Center Distributed Active Archive Center,
338 <https://doi.org/10.5067/3X5Q3X7Y87U3>, 2025.

339 Chen, J. Wu, Y., O'Connor, M., Cardenas, M. B., Schaefer, K., Michaelides, R., and Kling, G.: Active layer freeze-thaw and
340 water storage dynamics in permafrost environments inferred from InSAR, *Remote Sensing of Environment*, 248, 112007,
341 <https://doi.org/10.1016/j.rse.2020.112007>, 2020.

342 Daniels, D. J. (Ed): *Ground Penetrating Radar, Volume 1*, The Institution of Electrical Engineers, 2004.

343 Duquette, L. S.: Snow Characteristics along Caribou Trails and within Feeding Areas during Spring Migration, *Arctic*, 41,
344 143-144, <https://journalhosting.ucalgary.ca/index.php/arctic/article/view/64760/48674>, 1988.

345 Eppler, J., Rabus, B., and Morse, P.: Snow water equivalent change mapping from slope-correlated synthetic aperture radar
346 interferometry (InSAR) phase variations, *The Cryosphere*, 16, 1497–1521, <https://doi.org/10.5194/tc-16-1497-2022>, 2022.

347 Fair, Z., Vuyovich, C., Neumann, T. A., Larsen, C. F., Stuefer, S. L., Mason, M., and May, L: Characterizing ICESat-2 Snow
348 Depths Over the Boreal Forests and Tundra of Alaska in Support of the SnowEx 2023 Campaign, *Water Resources Research*,
349 61, e2024WR039076, [https://essopenarchive.org/users/524768/articles/1233703-characterizing-icesat-2-snow-depths-over-](https://essopenarchive.org/users/524768/articles/1233703-characterizing-icesat-2-snow-depths-over-the-boreal-forests-and-tundra-of-alaska-in-support-of-the-snowex-2023-campaign)
350 [the-boreal-forests-and-tundra-of-alaska-in-support-of-the-snowex-2023-campaign](https://essopenarchive.org/users/524768/articles/1233703-characterizing-icesat-2-snow-depths-over-the-boreal-forests-and-tundra-of-alaska-in-support-of-the-snowex-2023-campaign), 2025.

351 Jorgensen, T., Yoshikawam K., Kanevskiy, M., Shur, Y., Romanovsky, V., Marchenko, S., Grosse, G., Brown, J., and Jones,
352 B.: Permafrost Characteristics of Alaska [map]
353 https://permafrost.gi.alaska.edu/sites/default/files/AlaskaPermafrostMap_Front_Dec2008_Jorgenson_etal_2008.pdf, 2008.

354 Kelsey, K. C., Pedersen, S. H., Leffler, A. J., Sexton, J. O., Feng, M., and Welker, J. M.: Winter snow and spring temperature
355 have differential effects on vegetation phenology and productivity across Arctic plant communities, *Global Change Biology*,
356 27, 1572–1586, <https://doi.org/10.1111/gcb.15505>, 2021.

357 Kovacs, A., Gow, A. J., and Morey, R. M.: The in-situ dielectric constant of polar firn revisited, *Cold Regions Science and*
358 *Technology*, 23, 245–256, [https://doi.org/10.1016/0165-232X\(94\)00016-Q](https://doi.org/10.1016/0165-232X(94)00016-Q), 1995.

359 Larsen, C.: SnowEx23 Airborne Lidar-Derived 0.25M Snow Depth and Canopy Height, Version 1 [data set], NASA National
360 Snow and Ice Data Center Distributed Active Archive Center, <https://doi.org/10.5067/BV4D8RRU1H7U>, 2024.

361 Mason, M., Vuyovich, C. M., Stuefer, S., Elder, K., Vas, D., Marshall, H., and Durand, M.: SnowEx23 Mar23 Snow Pit
362 Measurements, Version 1 [data set], NASA National Snow and Ice Data Center Distributed Active Archive Center,
363 <https://doi.org/10.5067/SJZ90KNPKCYR>, 2024

364 May, L. D., Stuefer, S. L., Goddard, S. D., and Larsen, C. F.: Analyzing vegetation effects on snow depth variability in Alaska’s
365 boreal forests with airborne lidar, *The Cryosphere*, 19, 3477-3492, <https://doi.org/10.5194/tc-19-3477-2025>, 2025.

366 McGrath, D., Webb, R., Shean, D., Bonnell, R., Marshall, H.-P., Painter, T. H., Molotch, N. P., Elder, K., Hiemstra, C., and
367 Brucker, L.: Spatially Extensive Ground-Penetrating Radar Snow Depth Observations During NASA’s 2017 SnowEx
368 Campaign: Comparison With In Situ, Airborne, and Satellite Observations, *Water Resources Research*, 55, 10026–10036,
369 <https://doi.org/10.1029/2019WR024907>, 2019.

370 Meehan, T. G. and Rowland, T.: SnowEx23 CRREL Ground Penetrating Radar, Version 1 [data set], NASA National Snow
371 and Ice Data Center Distributed Active Archive Center, <https://doi.org/10.5067/TSU0U7L4X2UW>, 2024.

372 Meehan, T. G., Hojatimalekshah, A., Marshall, H.-P., Deeb, E. J., O’Neel, S., McGrath, D., Webb, R. W., Bonnell, R., Raleigh,
373 M. S., Hiemstra, C., and Elder, K.: Spatially distributed snow depth, bulk density, and snow water equivalent from ground-
374 based and airborne sensor integration at Grand Mesa, Colorado, USA, *The Cryosphere*, 18, 3253–3276,
375 <https://doi.org/10.5194/tc-18-3253-2024>, 2024.

376 Meredith, M., Sommerkorn, M., Cassotta, S., Derksen, C., Ekaykin, A., Hollowed, A., Kofinas, G., Mackintosh, A.,
377 Melbourne-Thomas, J., Muelbert, M. M. C., Ottersen, G., Pritchard, H., and Schuur, E. A. G.: Polar Regions. IPCC Special
378 Report on the Ocean and Cryosphere in a Changing Climate, 203-320, <https://doi.org/10.1017/9781009157964.005>, 2019.

379 NASA Earth Observatory: Forest on the Threshold, [blog post].
380 https://earthobservatory.nasa.gov/features/BorealThreshold/boreal_threshold4.php, 2006.

381 Obu, J., Westermann, S., Bartsch, A., Berdnikov, N., Christiansen, H. H., Dashtseren, A., Delaloye, R., Elberling, B.,
382 Etzelmüller, B., Kholodov, A., Khomutov, A., Kääb, A., Leibman, M. O., Lewkowicz, A. G., Panda, S. K., Romanovsky, V.,
383 Way, R. G., Westergaard-Nielsen, A., Wu, T., Yamkhin, J., and Zou, D.: Northern Hemisphere permafrost map based on
384 TTOP modelling for 2000–2016 at 1 km² scale, *Earth-Science Reviews*, 193, 233-316,
385 <https://doi.org/10.1016/j.earscirev.2019.04.023>, 2019.

386 Pedersen, S. H., Bentzen, T. W., Reinking, A. K., Liston, G. E., Elder, K., Lenart, E. A., Prichard, A. K., and Welker, J. M.:
387 Quantifying effects of snow depth on caribou winter range selection and movement in Arctic Alaska, *Movement Ecology*, 9,
388 48, <https://doi.org/10.1186/s40462-021-00276-4>, 2021.

389 Penczykowski, R. M., Connolly, B. M., and Barton, B. T.: Winter is changing: Trophic interactions under altered snow
390 regimes, *Food Webs*, 13, 80–91, <https://doi.org/10.1016/j.fooweb.2017.02.006>, 2017.

391 Pomeroy, J. W. and Li, L.: Prairie and arctic areal snow cover mass balance using a blowing snow model, *Journal of*
392 *Geophysical Research: Atmospheres*, 105, 26619-26634, <https://doi.org/10.1029/2000JD900149>, 2000.

393 Pruitt, W. O., Jr. (1970) Some ecological aspects of snow, *Ecology of the Subarctic Regions: Proceedings of the Helsinki*
394 *Symposium*, UNESCO, 83-99, <https://unesdoc.unesco.org/ark:/48223/pf0000004082>, 1970.

395 Stuefer, S. L., Hale, K., May, L. D., Mason, M., Vuyovich, C., Marshall, H. P., Vas, D., and Elder, K.: Snow depth
396 measurements from Arctic tundra and boreal forest collected during NASA SnowEx Alaska Campaign, *Scientific Data*, 12,
397 919, <https://doi.org/10.1038/s41597-025-05430-w>, 2025.

398 Sturm, M. and Liston, G. E.: Revisiting the Global Seasonal Snow Classification: An Updated Dataset for Earth System
399 Applications, <https://doi.org/10.1175/JHM-D-21-0070.1>, 2021.

400 Vuyovich, C., Stuefer, S., Gleason, K., Durand, M., Marshall, H. P., Osmanoglu, B., Elder, K., Vas, D., Mason, M., Nolin, A.,
401 Youcha, E., Gelvin, A., Larsen, C., Pedersen, S., Hodkinson, D., Deeb, E., and Boyd, D.: NASA SnowEx 2023 Experiment

402 Plan [science plan], <https://snow.nasa.gov/sites/default/files/users/user354/SNEX->
403 [Campaigns/2023/NASA_SnowEx_Experiment_Plan_2023_draft_20June2024.pdf](https://snow.nasa.gov/sites/default/files/users/user354/SNEX-Campaigns/2023/NASA_SnowEx_Experiment_Plan_2023_draft_20June2024.pdf), 2024.

404 Webb, R.: SnowEx23 University of Wyoming Ground Penetrating Radar, Version 1 [data set]. NASA National Snow and Ice
405 Data Center Distributed Active Archive Center, <https://doi.org/10.5067/H3D9IT1W6JT6>, 2024.

406

407